BENTHAM SCIENCE

CrossMark

Current Medical Imaging

Content list available at: https://benthamscience.com/journals/cmir

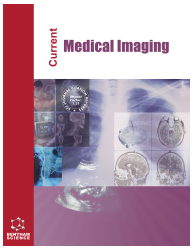

RESEARCH ARTICLE

Discrimination between Benign and Malignant Lung Lesions using Volumetric Quantitative Dynamic Contrast-enhanced MRI

Fang Wei[1], Fu Weidong[1], Zhou Wenming[1,*], He Lei[1], Cheng Xiaosan[1], Mao Zhongliang[1], Liu Qianyun[1] and Lin Huashan[2]

[1]*Department of Radiology, The Central Hospital of Yueyang, Yueyang 414000, China*
[2]*Department of Pharmaceuticals Diagnosis, GE Healthcare, Changsha 410005, China*

Abstract:

Background:

Dynamic contrast-enhanced magnetic resonance imaging (DCE-MRI) is considered a promising method in lung lesion assessment.

Methods:

Sixty-four patients with single pulmonary lesions (SPLs) received DCE-MRI at 3.0 T. Of them, 49 cases were diagnosed with lung cancer, and 15 with benign pulmonary nodules (8 inflammatory nodules, 5 tuberculosis, and 2 abscesses). SPLs were quantitatively analyzed to determine the pulmonary lesions-related perfusion parameters, including reflux constant (Kep), volume transfer constant (K_{trans}), the maximum slope of increase (MaxSlope), extravascular extracellular space volume fraction (Ve), apparent diffusion coefficient (ADC), the initial area in the signal intensity-time curve (IAUGC), and contrast-enhancement ratio (CER). In addition, a Student's t-test was conducted to calculate statistical significance regarding the quantitatively analyzed perfusion parameters in benign SPLs compared to malignant SPLs. The area under (AUC) the receiver operating characteristic (ROC) curve was studied to investigate the performance of perfusion parameters in diagnosing lung cancer.

Results:

Values of K_{trans}, Kep, Ve, MaxSlope, and IAUGC increased within malignant nodules relative to benign nodules (K_{trans}: 0.21 ±0.08 *vs*. 0.73 ±0.40, P = 0.0001; Kep: 1.21 ±0.66 *vs*. 1.83 ±0.90, P = 0.0163; Ve: 0.24 ±0.08 *vs*. 0.47 ±0.18, P < 0.0001; MaxSlope: 0.09 ±0.14 *vs*. 0.28 ±0.29, P = 0.0166; IAUGC: 0.18 ±0.09 *vs*. 0.55 ±0.34, P = 0.0001). Meanwhile, malignant nodules presented higher ADC than benign nodules (0.0016 ±0.0006 *vs*. 0.0012 ±0.0003, P = 0.0019). K_{trans} and IAUGC showed the best diagnostic performance with AUCs [1.0, 95%CI (0.99–1.0); 0.93, 95%CI(0.85–1.0), respectively].

Conclusion:

Malignant pulmonary lesions had higher values of K^{trans}, Ve, Kep, MaxSlope, and IAUGC compared to benign pulmonary lesions. Overall, perfusion parameters of DCE-MRI facilitate discrimination between benign from malignant pulmonary nodules.

Keywords: Dynamic contrast-enhanced magnetic resonance imaging, Lung lesions, Single pulmonary lesion (SPL), Diagnosis, AUC, ADC.

Article History	Received: November 09, 2022	Revised: June 22, 2023	Accepted: July 01, 2023

1. BACKGROUND/INTRODUCTION

Lung cancer belongs to a multi-step and multi-factorial illness, is the most fatal cancer worldwide, and has several histological subtypes [1]. The etiology behind lung cancer remains poorly reported. Smoking and air pollution have been proven to be two key risk factors. Other risk factors, including occupational exposure (asbestos), also contribute to lung cancer development [2]. Lung cancer morbidity among the Chinese people has rapidly increased recently, severely challenging the health of mankind [3].

Computed tomography (CT) has become the most commonly used technique in assessing pulmonary lesions, and ^{18}F-fluorodeoxyglucose positron-emission tomography (PET)-

* Address correspondence to this author at the Department of Radiology, The Central Hospital of Yueyang, 39# Maoling East Road, Yueyang 414000, Hunan Province, China; Tel/Fax: +86-0730-8246400; E-mail: ct8246400@163.com).

CT has often been employed for a definitive diagnosis [4, 5]. Multiple solitary pulmonary lesions (SPLs) still exist that exhibit atypical traits, encompassing infectious and inflammatory disorders, like inflammatory myofibroblastic tumors, granuloma, and active tuberculosis [6, 7]. Additionally, CT and PET-CT increase the radiation burden. Thus, another thorough evaluation should be done to check SPLs' inner microstructure in a non-invasive manner.

Currently, magnetic resonance imaging (MRI) is applied to diagnose tumors in various organs. DCE-MRI is usually confronted with problems, such as inadequate scanning speed and motion artifacts. Moreover, it is also a robust tool for diagnosing lung cancers [8, 9], with equivalent or superior performance compared to PET [10]. Thus, the free-breathing DCE-MRI with high acceleration has great practical significance to lung examinations.

Conventional MRI can provide significant lung lesions-related information, such as size, number, and location of lesions; however, it remains insufficient in diagnosing malignant lesions and differentiating between histologic subtypes. DCE-MRI provides functional information concerning tumors and reflects hemodynamic variations in cancer treatment. Under the two-compartment model [11], DCE-MRI can provide the following pharmacokinetic parameters: (i) volume transfer constant (Ktrans), (ii) extravascular extracellular space per unit tissue volume (Ve), (iii) plasmatic volume per unit of tissue volume (Vp), (iv) rate constant (Kep), *i.e.*, the Kt^{rans}/Ve ratio. Different from traditional imaging, DCE-MRI performs a quantitative assessment of tumor microvasculature by measuring multiple parameters that reflect specific physiologic features like Ktrans. Patients with acute and subacute cerebral infarction showed greater Ktrans value than those without cerebrovascular events [12]. Breast cancer exhibiting greater Ktrans on DCE-MRI is attributed to bad histopathologic diagnostic factors [13]. DCE-MRI perfusion parameters are promising biomarkers in evaluating tumor prognosis and angiogenesis.

Considering the aforementioned studies, we hypothesized that early changes in DCE-MRI parameters might contribute to the evaluation of pulmonary lesions. This study used DCE-MRI to examine the diagnostic accuracy of pharmacokinetic parameters for pulmonary lesions.

2. METHODS

2.1. Patients

The prospective research was approved by the Medical Ethics Committee of The Central Hospital of Yueyang (No. YY2021-018) and performed in accordance with the Declaration of Helsinki. Prior informed consent was obtained from each participant. Between January, 2020, and January, 2021, 71 cases having indeterminate SPLs confirmed by CT were included in the study. The following were inclusion criteria: (a) Cases without any prior therapy, (b) Short-axis diameter >1 cm on CT, (c) No MRI contraindication, and (d) Patients with a histopathologically confirmed diagnosis within 21 days following MRI. This study excluded three patients showing motion artifact-caused unsatisfactory imaging quality and four patients due to inadequate histopathological confirmation. Finally, 64 patients were diagnosed by pathological examination operatively.

2.2. MRI

MRI was performed using a 3.0 T GE Discovery 750 MRI system (GE Healthcare HDx MR, Waukesha, USA) plus the 8-channel cardiovascular phased-array coil. Data were obtained from free-breathing using the following imaging parameters: in-plane matrix = 256 × 256, in-plane field of view (FOV) = 300 × 300 mm^2, in-plane spatial resolution = 1.25 × 1.25 mm^2, slice number = 40, acquired slice thickness = 5 mm, flip angle = 12°, bandwidth = 580 Hz/voxel, and TR/TE = 3.40 ms/1.64 ms. To obtain 22 partitions, 90% partial Fourier was used in slice dimension; each image was interpolated into 40 partitions after reconstruction to obtain a 3-mm thick interpolated slice. In total, 3000 radial spokes were obtained from every partition, with the overall scanning time lasting 281 s. In every scan, patients had to maintain normal and consistent breathing and avoid abrupt deep breathing. The fat-suppressed breath-hold axial T1W volume interpolated gradient-echo liver acquisition and volume acceleration (LAVA) sequence was employed to gather DCE-MRI data. After acquiring the preference mask, we injected a weight-based full dose (0.1 mmol/kg) of gadobenate dimeglumine (Gd-BOPTA, MultiHance, Bracco SpA, Milano, Italy) at 2.0 mL/s and used a power injector to supplement 20 mL of saline flush. DCE-MRI images were obtained at 5 s upon injection of the contrast agent, and 15 dynamic phases were obtained every 10 s from the patients.

2.3. Post-processing of MRI Data

In this study, two radiologists (F.W. and Z.W., having five-year and ten-year MRI experience, respectively, and unaware of histopathological outcomes) conducted data analysis using a consensus approach. F.W. delineated the region of interest (ROI) manually for a solid lesion in the central section in the longest diameter with a view to avoiding visible vessels, liquefaction, or necrosis. Plotted ROIs were moved to DCE-MRI maps.

2.4. Quantitatively Analyzed Perfusion Parameters for DCE-MRI

Using the two-compartment model, DCE-MRI can offer multiple pharmacokinetic parameters. Lesion volume (cm^3), arterial input function (AIF), and kinetic parameters were determined by using the quantitative analysis software GenIQ (GE Healthcare). Thereafter, Ve, Kep, Ktrans, and other parameters were computed automatically based on the concentration curve and fitted model. The average pixel parameters in ROI were documented. Ktrans refers to the volume transfer constant indicating the plasma-to-EES transfer of the contrast agent (min^{-1}). Kep indicates the rate constant representing EES-plasma transfer of contrast agent (min^{-1}). Ve = Ktrans/Kep denotes EES volume per unit of tissue volume.

The following semiquantitative parameters for DCE-MRI were derived based on signal intensity–time curve images: the maximum slope of increase (MaxSlope; mmol/s), *i.e.*, the slope

in the steepest part under the concentration curve, the contrast-enhancement ratio (CER) = (peak signal-baseline signal)/(baseline signal), the bolus arrival time (BAT) = the time (in seconds) from contrast injection to tracer bolus arrival for the lesion, and the initial area of the signal intensity–time curve (IAUGC) = the area under the tissue concentration curve from BAT to 60 s from contrast injection)/(area under the AIF concentration curve from BAT to 60 s from contrast injection). Fig. (**1**) exhibits DCE-MRI parameters obtained for the diagnosis of a patient with left upper lung adenocarcinoma.

2.5. Statistical Analyses

Qualitative variables were examined using Pearson's chi-square test and Fisher's exact test, while Student's t-test, analysis of variance or Mann-Whitney test were performed to evaluate quantitative parameters. A ROC curve was drawn to evaluate diagnostic significance. Statistical analysis was done using R (version 4.0.1). Each statistical test was two-sided, with a P-value <0.05 indicating statistical significance.

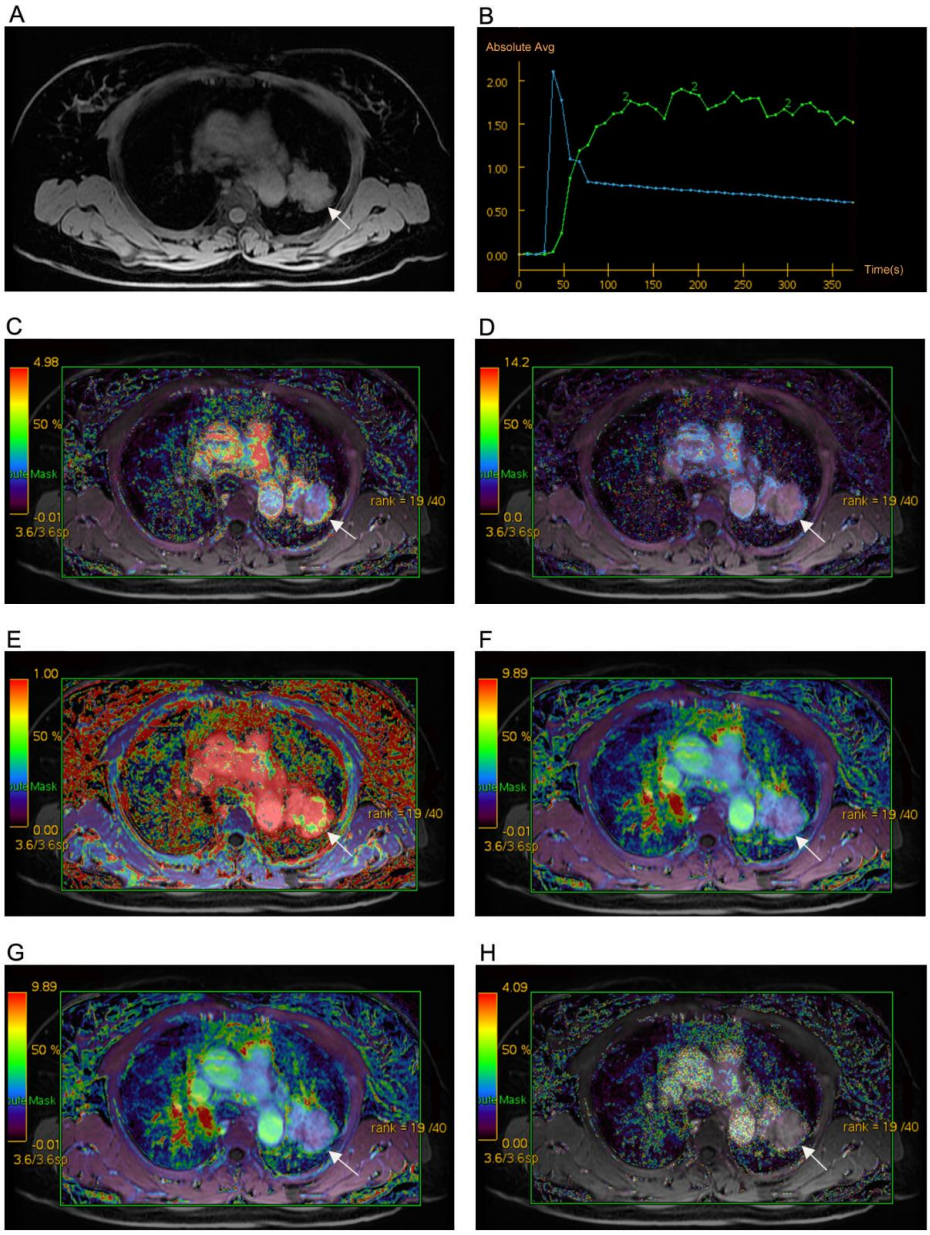

Fig. (1). DCE-MRI parameters obtained during the diagnosis of a patient with left upper lung adenocarcinoma. The determined DCE-MRI parameters: (**A**). T1-weighed, (**B**). time-concentration curve, (**C**). pseudo-color map of Ktrans, (**D**). pseudo-color map of Kep, (**E**). pseudo-color map of Ve, (**F**). pseudo-color map of CER, (**G**). pseudo-color map of IAUGC, (**H**). pseudo-color map of MaxSlope.

Table 1. Clinic and DCE-MRI parameters in lung nodules.

Variables	Nature of Lung Nodules		P value [a]
-	Benign	Malignant	-
Gender	-	-	-
Male	11	35	0.854
Female	4	14	-
Age	62.53±9.11	62.27±7.15	0.906
Size (mm)	31.73±23.47	45.96±20.81	**0.028**
Ktrans	0.21±0.08	0.73±0.40	**<0.001**
Ve	0.24±0.08	0.47±0.18	**<0.001**
Kep	1.21±0.66	1.83±0.90	**0.016**
MaxSlope	0.09±0.14	0.28±0.29	**0.017**
CER	3.48±4.25	3.47±3.48	0.987
IAUGC	0.18±0.09	0.55±0.34	**<0.001**
ADC	0.0016±0.0006	0.0012±0.0003	**0.002**

Note: DCE-MRI dynamic contrast enhanced magnetic resonance imaging. Patients were segregated into benign/malignant groups.
[a] Statistical analysis were performed with Fisher exact test or T-testing method.

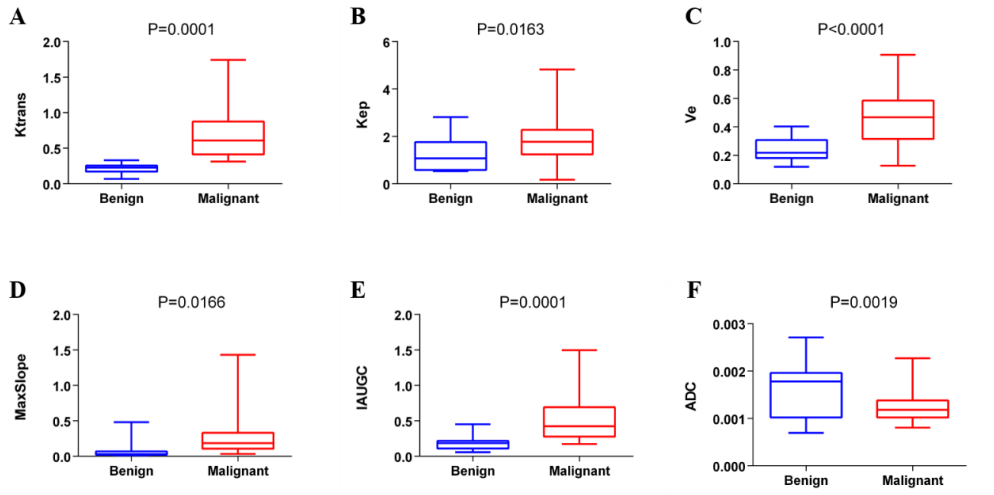

Fig. (2). DCE-MRI parameters distinguish lung cancers from benign nodules. (**A**). Ktrans, *P* = 0.0001, (**B**). Kep, *P* = 0.0163, (**C**). Ve, *P*<0.0001, (**D**). MaxSlope, *P* = 0.0166, (**E**). IAUGC, *P* = 0.0001, (**F**). ADC, P = 0.0019.

3. RESULTS

3.1. Basic Features of the Patients

In total, sixty-four cases were included (benign group (n = 15), malignant group (n = 49). The clinical features and DCE-MRI parameters of both groups are summarized and compared in Table **1**. Gender and age data showed no significant difference. Malignant lesions were greater in size compared to benign lesions (31.73 ±23.47 *vs*. 45.96 ±20.81 mm, P = 0.028). In comparison with the benign group, malignant group patients showed significantly different perfusion parameters (with an increase in Ktrans, Ve, Kep, MaxSlope, and IAUGC and a decrease in ADC values) (Table **1**).

3.2. The Potential of MRI Parameters in Diagnosing Lung Nodules

The associations between DCE-MRI parameters and malignant nodules were examined (Fig. **2**). The Ktrans, Kep, Ve, MaxSlope, and IAUGC values of malignant nodules were greater than those of benign lesions (Ktrans: 0.21 ±0.08 *vs*. 0.73 ±0.40, P = 0.0001; Kep: 1.21 ±0.66 *vs*. 1.83 ±0.90, P = 0.0163; Ve: 0.24 ±0.08 *vs*. 0.47 ±0.18, P < 0.0001; MaxSlope: 0.09 ±0.14 *vs*. 0.28 ±0.29, P = 0.0166; IAUGC: 0.18 ±0.09 *vs*. 0.55 ±0.34, P = 0.0001). Also, malignant nodules presented higher ADC than benign nodules (0.0016 ±0.0006 *vs*. 0.0012 ±0.0003, P = 0.0019). However, CER values were comparable in benign and malignant nodules with no statistical significance (Table **1**). ROC curves were exhibited, and AUCs were obtained to quantify the discrimination efficiency in diagnosing lung cancers (Fig. **3**). Ktrans and IAUGC show the best diagnostic performance with AUCs (1.0, 95%CI(0.99–1.0); 0.93, 95%CI(0.85–1.0), respectively) in the current study.

For investigating DCE-MRI parameters' clinicopathological impacts on lung cancers, an experiment was conducted to examine the correlation of specific

parameters with other clinical parameters in 49 patients with lung cancer. Table **2** presents the correlation of Kep to the size of tumors. In addition, the association of DCE-MRI measures with a subtype of malignant nodules was evaluated (Fig. **4**). The malignant nodules were confirmed to be adenocarcinoma (AC, n = 26), squamous cell carcinoma (SCC, n = 16), small cell lung cancer (SCLC, n = 5), (SC, n = 1), and mixed squamous adenocarcinoma (n = 1). SC and mixed squamous adenocarcinoma were not included because of only one patient in the group. Kep values and MaxSlope seemed higher among AC patients than SCC patients. No significant correlations were observed between the subtype of lung cancer and other DCE-MRI parameters, including Ktrans, Ve, Kep, MaxSlope, CER, IAUGC, and ADC (Table **3**).

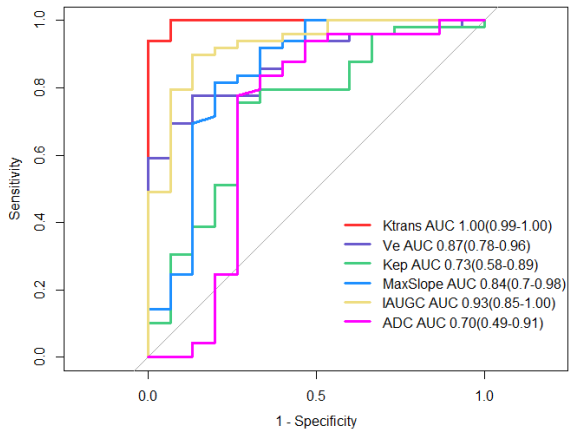

Fig. (3). Receiver operating characteristics (ROC) curves and area under curves (AUCs) for diagnosis of lung cancers using Ktrans, Ve, Kep, MaxSlope, IAUGC, and ADC parameters.

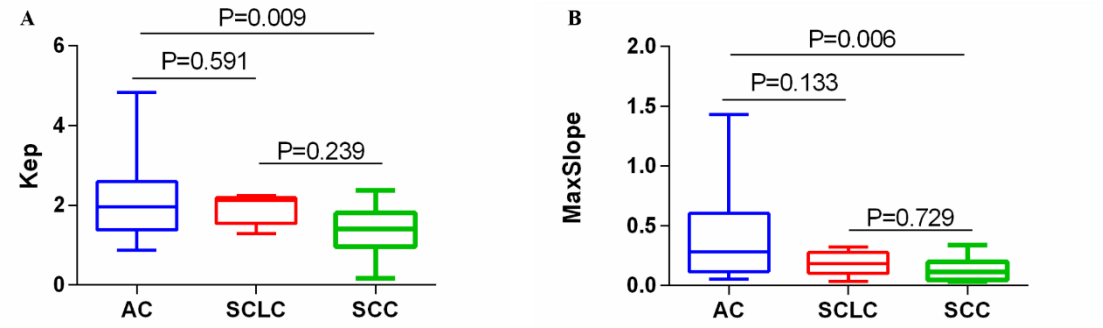

Fig. (4). The relative levels of DCE-MRI parameters among three lung cancer subtypes: AC (n = 26), SCLC (n = 5), and SCC (n = 16). (**A**). Kep; (**B**), MaxSlope.

Table 2. The correlation between clinic features and DCE-MRI parameters in lung cancers.

Variables	Number	Ktrans		Ve		Kep		MaxSlope		CER		IAUGC	
		R	P value[a]	R	P value[a]	R	P value[a]	R	P value[a]	R	P value[a]	R	P value[a]
Gender	49	0.399	0.004*	0.428	0.002*	0.157	0.283	0.428	0.002*	0.173	0.236	0.383	0.007*
Age	62.04±7.21	0.121	0.409	0.018	0.904	0.173	0.235	0.236	0.102	0.216	0.136	0.155	0.286
Smoking	49	-0.263	0.068	-0.244	0.091	-0.197	0.174	-0.427	0.002*	-0.188	0.196	-0.235	0.104
Tumor location	49	0.043	0.767	0.052	0.722	-0.197	0.176	-0.357	0.012*	-0.396	0.005*	0.055	0.708
Tumor number	49	-0.142	0.332	0.063	0.665	-0.358	0.012*	0.075	0.611	-0.007	0.959	-0.101	0.491
Size (mm)	45.21±20.90	-0.203	0.163	0.060	0.684	-0.480	0.000*	-0.436	0.002*	-0.479	0.001*	-0.065	0.655
Tumor differentiation	49	0.198	0.172	0.085	0.563	0.235	0.104	0.204	0.159	0.125	0.391	0.118	0.419
Lymphatic metastasis	49	0.003	0.984	0.053	0.718	-0.214	0.139	-0.270	0.060	-0.443	0.001*	0.081	0.581
Vascular invasion	49	-0.077	0.599	0.121	0.406	-0.373	0.008*	-0.233	0.108	-0.155	0.286	0.053	0.716
CEA	44	0.379	0.011*	0.277	0.069	0.113	0.466	0.182	0.237	-0.033	0.833	0.322	0.033*

(Table 2) contd.....

Variables	Number	Ktrans		Ve		Kep		MaxSlope		CER		IAUGC	
		R	P value[a]	R	P value[a]	R	P value[a]	R	P value[a]	R	P value[a]	R	P value[a]
CA125	44	-0.152	0.324	-0.023	0.881	-0.299	0.048*	-0.138	0.372	-0.242	0.114	-0.038	0.808
CA199	44	0.002	0.989	0.122	0.430	-0.206	0.179	-0.131	0.397	-0.273	0.073	-0.011	0.943
SCCA	39	-0.014	0.932	0.084	0.610	-0.197	0.230	-0.173	0.291	-0.433	0.006*	0.026	0.876
CYFRA21-1	34	0.112	0.529	0.441	0.009*	-0.329	0.057	0.148	0.403	0.020	0.912	0.224	0.203

Note: DCE-MRI dynamic contrast enhanced magnetic resonance imaging; CEA carcinoembryonic antigen; CA125 carbohydrate antigen 125; CA199 carbohydrate antigen 125; SCCA squamous cell carcinoma antigen; CYFRA21-1 Cytokeratin-19-fragment.

[a] Statistical analysis were performed with Pearson Test or Spearman Test.

*: P< 0.05.

Table 3. Clinic and DCE-MRI parameters in three subtypes of lung cancers.

Variables	Types of lung cancer			P value[a]
	AC	SCC	SCLC	-
Gender	-	-	-	-
Male	13	16	4	0.001
Female	13	0	1	-
Age	61.92±7.38	61.94±7.56	63.00±6.44	0.954
Size	37.62±18.20	56.19±17.65	49.60±30.08	0.014
Ktrans	0.86±0.46	0.57±0.25	0.61±0.30	0.064
Ve	0.51±0.20	0.43±0.12	0.36±0.16	0.144
Kep	2.14±1.04	1.39±0.56	1.92±0.39	0.030
MaxSlope	0.40±0.36	0.14±0.11	0.19±0.10	0.015
CER	4.10±3.90	2.99±3.41	2.23±0.42	0.430
IAUGC	0.65±0.41	0.43±0.17	0.42±0.23	0.088
ADC	0.0012±0.003	0.0013±0.0003	0.0011±0.0.0003	0.379

Note: DCE-MRI dynamic contrast enhanced magnetic resonance imaging.

AC, adenocarcinoma; SCC, squamous cell carcinoma; SCLC, small cell lung cancer.

[a] Statistical analysis were performed with oneway anova test or Fisher' test.

4. DISCUSSION

Over the recent years, quantitative perfusion parameters with DCE-MRI have been proven underlying techniques to differentiate benign and malignant lesions [6, 14, 15]. We demonstrated obvious differences with regard to Ktrans, Ve, MaxSlope, IAUGC, and ADC of DCE-MRI between benign and malignant SPLs. The feasibility and performance of DCE-MRI were examined in simultaneous quantitative evaluation for pulmonary lesions.

DCE-MRI pharmacokinetics shows promising prospects in differential diagnosis for renal tumors, especially in the characterization of renal cell carcinoma subtype [16]. DCE-MRI parameters may be adopted for distinguishing malignant and benign breast lesions. Ktrans, Kep, and MaxSlope parameters serve as independent predictive factors for breast cancer, and DCE-MRI improves the diagnostic accuracy for breast malignancy [15]. Chen *et al*. (2018) reported that Ve and Ktrans in malignant lesions increased compared to benign lesions [17]. These findings conform well to the perfusion parameters obtained in the current study, where Ktrans and Ve values are greater in malignant lesions than in benign lesions. Ktrans shows a positive correlation with surface area, blood flow, and endothelial permeability. Higher Ktrans values indicate an increase in vascular permeability in disease progression like malignancy [14]. CER negatively correlated with size and lymphatic metastasis. The larger the tumor, the greater the likelihood of tumor necrosis that causes decreased CER. Furthermore, the current study suggests significant differences in MaxSlope, IAUGC, and ADC values in benign nodules compared to malignant pulmonary nodules, as determined using DCE-MRI; such results are not reported in earlier studies. Our study also highlights significant differences between MaxSlope and Kep among subtypes of lung cancers.

CONCLUSION

Overall, this research verifies the performance of quantitative evaluation for SPLs with the DCE-MRI technique. It shows significant differences in different parameters of DCE-MRI, such as Ktrans, Ve, MaxSlope, IAUGC, ADC, and CER, between benign and malignant nodules. It suggests the underlying effects of DCE-MRI on the preoperative identification of SPLs, including better surgical resection and reduced recurrence risk.

AUTHORS' CONTRIBUTIONS

W.F. and Wd.F. designed research, W.F., Z.M., Q.L., and H.L. collected data, W.F. and L.H. analyzed the data, W.F., W.Z., and L.H. wrote the main manuscript text, W.F. Z.M., and X.C. prepared figures and tables. All authors reviewed the manuscript.

LIST OF ABBREVIATIONS

DCE-MRI = Dynamic contrast-enhanced magnetic resonance imaging

SPL	=	Single pulmonary lesion
Kep	=	Reflux constant
K_{trans}	=	Volume transfer constant
MaxSlope	=	Maximum slope of increase
Ve	=	Extravascular extracellular space volume fraction
ADC	=	Apparent diffusion coefficient
IAUGC	=	Initial area in signal intensity-time curve
CER	=	Contrast-enhancement ratio
AUC	=	The area under the receiver operating characteristic
ROC	=	Receiver operating characteristic
CT	=	Computed tomography
PET	=	Positron-emission tomography
MRI	=	Magnetic resonance imaging
Vp	=	Plasmatic volume per unit of tissue volume
FOV	=	Field of view
LAVA	=	Liver acquisition and volume acceleration
Gd-BOPTA	=	Gadobenate dimeglumine
ROI	=	Region of interest
AIF	=	Arterial input function
BAT	=	Bolus arrival time
AC	=	Adenocarcinoma
SCC	=	Squamous cell carcinoma
SCLC	=	Small cell lung cancer

ETHICS APPROVAL AND CONSENT TO PARTICIPATE

The prospective research was approved by the Medical Ethics Committee of The Central Hospital of Yueyang. Prior informed consent was obtained from each participant.

HUMAN AND ANIMAL RIGHTS

No animals were used in this research. All procedures performed in studies involving human participants were in accordance with the ethical standards of institutional and/or research committee and with the 1975 Declaration of Helsinki, as revised in 2013.

CONSENT FOR PUBLICATION

Prior informed consent was obtained from each participant.

STANDRADS OF REPORTING

STROBE guidelines were followed.

AVAILABILITY OF DATA AND MATERIALS

The datasets used and/or analysed during the current study are available from the corresponding author [Z.W] upon reasonable request.

CONFLICT OF INTEREST

The authors declare that they have no competing interests, financial or otherwise.

FUNDING

The present work was funded by the Soft Science Research Project, 2019-37, Yueyang Technology Council, Hounan Province.

ACKNOWLEDGEMENTS

The authors would like to thank Dr. Zhourui Wang for his specialized consultation on the statistical analyses.

REFERENCES

[1] Siegel RL, Miller KD, Jemal A. Cancer statistics, 2019. CA Cancer J Clin 2019; 69(1): 7-34. [http://dx.doi.org/10.3322/caac.21551] [PMID: 30620402]

[2] Yang D, Liu Y, Bai C, Wang X, Powell CA. Epidemiology of lung cancer and lung cancer screening programs in China and the United States. Cancer Lett 2020; 468: 82-7. [http://dx.doi.org/10.1016/j.canlet.2019.10.009] [PMID: 31600530]

[3] Cao M, Chen W. Epidemiology of lung cancer in China. Thorac Cancer 2019; 10(1): 3-7. [http://dx.doi.org/10.1111/1759-7714.12916] [PMID: 30485694]

[4] Groheux D, Quere G, Blanc E, *et al.* FDG PET-CT for solitary pulmonary nodule and lung cancer: Literature review. Diagn Interv Imaging 2016; 97(10): 1003-17. [http://dx.doi.org/10.1016/j.diii.2016.06.020] [PMID: 27567555]

[5] O'Dowd EL, Baldwin DR. Lung cancer screening—low dose CT for lung cancer screening: recent trial results and next steps. Br J Radiol 2018; 91(1090): 20170460. [http://dx.doi.org/10.1259/bjr.20170460] [PMID: 28749712]

[6] Zhou SC, Wang YJ, Ai T, *et al.* Diagnosis of solitary pulmonary lesions with intravoxel incoherent motion diffusion-weighted MRI and semi-quantitative dynamic contrast-enhanced MRI. Clin Radiol 2019; 74(5): 409.e7-409.e16. [http://dx.doi.org/10.1016/j.crad.2018.12.022] [PMID: 30795843]

[7] Jin K, Wang K, Zhang H, *et al.* Solitary pulmonary lesion in patients with history of malignancy: Primary lung cancer or metastatic cancer? Ann Surg Oncol 2018; 25(5): 1237-44. [http://dx.doi.org/10.1245/s10434-018-6360-6] [PMID: 29417404]

[8] Serai SD, Rapp JB, States LJ, Andronikou S, Ciet P, Lee EY. Pediatric lung MRI: Currently available and emerging techniques. AJR Am J Roentgenol 2021; 216(3): 781-90. [http://dx.doi.org/10.2214/AJR.20.23104] [PMID: 33474982]

[9] Allen BD, Schiebler ML, Sommer G, *et al.* Cost-effectiveness of lung mri in lung cancer screening. Eur Radiol 2020; 30(3): 1738-46. [http://dx.doi.org/10.1007/s00330-019-06453-9] [PMID: 31748855]

[10] Chen GX, Wang MH, Zheng T, Tang GC, Han FG, Tu GJ. Diffusion: Weighted magnetic resonance imaging for the detection of metastatic lymph nodes in patients with lung cancer: A meta-analysis. Mol Clin Oncol 2017; 6(3): 344-54. [http://dx.doi.org/10.3892/mco.2017.1153] [PMID: 28451411]

[11] Li CH, Chen FH, Schellingerhout D, Lin YS, Hong JH, Liu HL. Flow *versus* permeability weighting in estimating the forward volumetric transfer constant (K^{trans}) obtained by DCE-MRI with contrast agents of differing molecular sizes. Magn Reson Imaging 2017; 36: 105-11. [http://dx.doi.org/10.1016/j.mri.2016.10.027] [PMID: 27989901]

[12] Wang GC, Chen YJ, Feng XR, Feng PY. Diagnostic value of HR□MRI and DCE□MRI in unilateral middle cerebral artery inflammatory stenosis. Brain Behav 2020; 10(9): e01732. [http://dx.doi.org/10.1002/brb3.1732] [PMID: 32767660]

[13] Kang SR, Kim HW, Kim HS. Evaluating the relationship between dynamic contrast□enhanced mri (dce-mri) parameters and pathological characteristics in breast cancer. J Magn Reson Imaging 2020; 52(5): 1360-73. [http://dx.doi.org/10.1002/jmri.27241] [PMID: 32524658]

[14] Kumar N, Sharma M, Aggarwal N, *et al.* Role of various DW MRI and DCE MRI parameters as predictors of malignancy in solid pulmonary lesions. Canadian Ass Radiol J 2021; 72(3): 525-32. [http://dx.doi.org/10.1177/0846537120914894]

[15] Cheng Z, Wu Z, Shi G, *et al.* Discrimination between benign and malignant breast lesions using volumetric quantitative dynamic contrast-enhanced MR imaging. Eur Radiol 2018; 28(3): 982-91. [http://dx.doi.org/10.1007/s00330-017-5050-2] [PMID: 28929243]

[16] Wang H, Su Z, Xu X, *et al.* Dynamic contrast-enhanced mri in renal tumors: Common subtype differentiation using pharmacokinetics. Sci

Rep 2017; 7(1): 3117.
[http://dx.doi.org/10.1038/s41598-017-03376-7] [PMID: 28596583]

[17] Chen L, Liu D, Zhang J, *et al.* Free-breathing dynamic contrast-enhanced MRI for assessment of pulmonary lesions using golden-angle radial sparse parallel imaging. J Magn Reson Imaging 2018; 48(2): 459-68.
[http://dx.doi.org/10.1002/jmri.25977] [PMID: 29437281]